

A Novel Robust 3-D Path Following Control for Keplerian Orbits*

Rodolfo Batista Negri[†] and Antônio F. B. de A. Prado

National Institute for Space Research, 12227-010, São José dos Campos, SP, Brazil

Abstract

This work proposes a novel path following control inspired in the famous two-body problem. In recognizing the mathematical structure of the two-body problem, we derive a robust path following law that is able to achieve any conic section, even for problems that do not involve inverse squared distance forces. In order to do so, we use the framework of the sliding mode control theory, which is only possible after we propose and prove asymptotic convergence of a new kind of sliding surface, specially suitable for this path following problem. With this new sliding surface, we are able to derive our control law, showing that it is asymptotic stable. The far range of applicability of this new path following is exemplified for three examples. A moving path following problem, in which a particle is requested to orbit an accelerated moving point, a patched hyperboles example, and an orbit keeping problem around the asteroid Itokawa. The control law derivation and the illustrative examples suggest that this path following strategy could have far reaching consequences in theoretical and practical researches.

1 Introduction

For the guidance of some crafts, it is often more interesting to apply path following control laws rather than reference tracking. Path following algorithms are most concerned in drive the craft to certain

geometry and keep on it therein, with no a priori time parameterization associated with the movement on the path. As opposed to reference tracking, which would make the craft converge to a specific point of the geometry in a predefined time. This advantage, among others [1, 3, 2, 4], make the path following control suitable for applications in the guidance problem of many different crafts: aircrafts [10, 14, 27], watercrafts [8, 33, 32], spacecraft [17], robots [29, 15, 16, 30]. In order to achieve path following, many different approaches have been proposed in the literature, such as using transverse feedback linearization [6, 20, 19], vector field [18, 31], and line-of-sight [11, 9]. Reference [25] make a survey of the different planar path following algorithms used for the guidance of UAVs (unmanned aerial vehicles).

Inspired in the two-body problem, this paper proposes a new strategy for the path following problem. Recognizing the integrals of motion which define the orbital geometry in the two-body problem[13] - eccentricity vector, angular momentum vector and energy -, we propose a new formulation in which these constants are the ones to be controlled. In this sense, we make our path following law formulated as a regulation problem of the angular momentum and eccentricity vectors. This allows any particle to describe a Keplerian orbit, with no need to be subjected to a central force field proportional to the inverse squared distance. To the best of our knowledge, this is a novelty in the literature. This makes our path following law applicable for many different scenarios and fields, such as to control underwater or aerial vehicles [21, 10, 14, 33, 32]. An obvious application is in problems already related to Keplerian motion, such

*Preprint. Under review.

[†]email: rodolfo.negri@inpe.br.

Personal website: rodolfobnegri.com

as to the autonomous orbit keeping problem [12].

Most of the applications that such path following could have are subject to disturbances, such as wind gusts, ocean current, or solar radiation pressure. For this reason, we formulate our path following law grounded on sliding mode control theory to achieve robust control. This is done by first representing the equations of motion of the particle in a radial-transverse-normal (RTN) frame, which is similar to the Frenet-Serret. We then propose a new way to write a sliding surface as a linear combination of radial and transverse components of each vector. We prove that this new sliding surface is asymptotically stable and asymptotically converge to the desired vector under certain conditions. This is very important as it allows to assign a single sliding surface for controlling a single vector. A consequence is that by doing so, we are able to control the plane of motion by a single sliding surface and control command, which could be interesting for further studies mixed with other planar algorithms [25]. We prove the asymptotic stability of our proposed control law and illustrate its validity for three different applications. One more generalist, considering the recently introduced and demanding moving path following (MPF) problem [23, 22], in which we assign a particle to describe an orbit around a point describing an accelerated sinusoidal trajectory, while also considering the point movement as a disturbance to the system. Secondly, a patched hyperboles example is showed, where the particle has to approach three different checkpoints. The last illustrative example considers the autonomous orbit keeping problem around the asteroid Itokawa, with the perturbation effects of solar radiation pressure, higher-order terms of the gravity field and unknown spin state.

2 Problem Statement

In order that the generality of the proposed control law be tractable we only consider the outer loop guidance of the vehicle center of mass, so we do not commit to any specific problem. We assume that the particle obeys the following equations of motion in an arbitrary Cartesian reference frame centred in the

point it will orbit:

$$\dot{\vec{r}}(t) = \vec{v}(t), \quad (1a)$$

$$\dot{\vec{v}}(t) = \vec{f}(\vec{r}, \vec{v}, t) + \vec{d}(\vec{r}, \vec{v}, t) + \vec{u}(\vec{r}, \vec{v}, t), \quad (1b)$$

in which $\vec{r}(t)$ and $\vec{v}(t) \in \mathbb{R}^{3 \times 1}$ are respectively the position and velocity vectors, $\vec{f}(\vec{r}, \vec{v}, t)$ is a smooth non-linear function of \vec{r} and \vec{v} representing a known dynamics, and $\vec{d}(\vec{r}, \vec{v}, t)$ is unknown or unmodelled disturbances that satisfy the following condition: $|d_j| \leq D_j$, where $D_j > 0$, $j = 1, 2, 3$.

We will derive our control laws in the radial-transverse-normal frame (RTN), which is a frame similar to the Frenet-Serret. In fact, a transposition between both frames can be obtained by a simply rotation around their normal axis. The RTN is a right-handed coordinate system in which the radial, transverse and normal components are defined accordingly to the particle's kinematics. The radial component is defined in the direction of the position vector \vec{r} , the normal component is perpendicular to the osculating plane in the direction of the specific angular momentum \vec{h} , and, finally, the transverse component completes the right-handed frame. Their versors are written as function of the particle's kinematics as:

$$\hat{r} = \frac{\vec{r}}{r}, \quad (2a)$$

$$\hat{\theta} = \hat{h} \times \hat{r}, \quad (2b)$$

$$\hat{h} = \frac{\vec{h}}{h}. \quad (2c)$$

Definition 2.1. An arbitrary Cartesian vector $\vec{A} \in \mathbb{R}^{3 \times 1}$ can be written in RTN as:

$$\vec{A}_{RTN} = \begin{bmatrix} A_R \\ A_T \\ A_N \end{bmatrix} = \begin{bmatrix} \vec{A} \cdot \hat{r} \\ \vec{A} \cdot \hat{\theta} \\ \vec{A} \cdot \hat{h} \end{bmatrix} = \begin{bmatrix} \hat{r}^T \\ \hat{\theta}^T \\ \hat{h}^T \end{bmatrix} \vec{A}, \quad (3)$$

in which the superscript \mathbb{T} represents the transverse, and the subscripts R , T and N stands for the radial, transverse and normal coordinates, respectively.

Using Definition 2.1, we can write the accelerations in Eqs. 1 in RTN as:

$$\vec{a}_{RTN} = \begin{bmatrix} f_R + u_R + d_R \\ f_T + u_T + d_T \\ f_N + u_N + d_N \end{bmatrix}. \quad (4)$$

The radial and transverse accelerations will act in the following equations of motion on the osculating plane:

$$\ddot{r} - r\dot{\theta}^2 = a_R, \quad (5a)$$

$$2\dot{r}\dot{\theta} + r\ddot{\theta} = a_T, \quad (5b)$$

in which θ is an angle representing the particle's position. Noting that the specific angular momentum can be represented as $h = r^2\dot{\theta}$, we can reduce the equations of motion to:

$$\ddot{r} = \frac{h^2}{r^3} + a_R, \quad (6a)$$

$$\dot{h} = ra_T \quad (6b)$$

The missing normal component is responsible for changing the osculating orbital plane. Its effect can be checked by obtaining the temporal variation of the specific angular momentum:

$$\dot{\vec{h}} = \vec{r} \times \vec{a} = ra_T \hat{h} - ra_N \hat{\theta}. \quad (7)$$

Because $\dot{\vec{h}} = \dot{h}\hat{h} + h\dot{\hat{h}}$, and using Eqs. 2 with a simple derivation similar to the one for obtaining polar coordinates, one can check that the RTN frame will follow the subsequent equations of motion:

$$\dot{\hat{r}} = \frac{h}{r^2} \hat{\theta}, \quad (8a)$$

$$\dot{\hat{\theta}} = \frac{ra_N}{h} \hat{h} - \frac{h}{r^2} \hat{r}, \quad (8b)$$

$$\dot{\hat{h}} = -\frac{ra_N}{h} \hat{\theta}. \quad (8c)$$

These are the equivalent to the Frenet-Serret formulas, but for RTN coordinates. To the best of our knowledge, although the RTN is extensively applied in astrodynamics and dynamical astronomy, this is the first time that its formulas equivalent to the Frenet-Serret are presented in the literature.

Definition 2.2. Consider an arbitrary vector \vec{A} written in a three-dimensional cartesian coordinate system. Also, consider this same vector written in RTN coordinates and represented as \vec{A}_{RTN} . We represent the derivative of \vec{A}_{RTN} with respect to time t , taken in each of its components, as $\frac{d}{dt}(\vec{A}_{RTN})$. While $\dot{\vec{A}}$, the time derivative of \vec{A} , is represented in RTN coordinates as $\dot{\vec{A}}_{RTN}$.

Thus, following Definition 2.2 and Eqs. 8, the time derivative of an arbitrary vector \vec{A}_{RTN} is:

$$\frac{d}{dt}(\vec{A}_{RTN}) = \begin{bmatrix} \dot{A}_R \\ \dot{A}_T \\ \dot{A}_N \end{bmatrix} = \begin{bmatrix} \dot{\vec{A}} \cdot \hat{r} + \frac{h}{r^2} A_T \\ \dot{\vec{A}} \cdot \hat{\theta} + \frac{ra_N}{h} A_N - \frac{h}{r^2} A_R \\ \dot{\vec{A}} \cdot \hat{h} - \frac{ra_N}{h} A_T \end{bmatrix} \quad (9)$$

3 Derivation of the law

In order to derive the control law, we need to make the following Assumption:

Assumption 3.1. *The particle's specific angular momentum and position vectors relative to the point to be orbited are such that $\vec{h} \neq 0$ and $\vec{r} \neq 0$.*

We are now able to make the proposition of a novel kind of sliding surface that will be central for our control derivation.

Proposition 3.1. *A sliding surface $s = 0$, $s \in \mathbb{R}$, written as a linear combination of the radial and transverse components of an arbitrary Cartesian vector $\vec{A} \in \mathbb{R}^{3 \times 1}$:*

$$s = A_T + \lambda A_R, \quad (10)$$

$\lambda > 0$, will asymptotically converge to $A_T = A_R = 0$, if $\dot{\vec{A}} = 0$.

Proof. From the first element of the vector in Eq. 9 it follows that:

$$A_T = \frac{1}{\dot{\theta}}(\dot{A}_R - \dot{\vec{A}} \cdot \hat{r}) \quad (11)$$

Because $\dot{\vec{A}} = 0$, the sliding surface s in Eq. 10 can be rewritten as:

$$s = \frac{1}{\dot{\theta}} \dot{A}_R + \lambda A_R = 0, \quad (12)$$

which has the following solution for the radial component of \vec{A} :

$$A_R(t) = A_R(t_0) e^{-\lambda(\theta(t) - \theta(t_0))} \quad (13)$$

But noting that $\dot{\theta} = h/r^2$, one find that:

$$\theta(t) - \theta(t_0) = \int_{t_0}^t \frac{h(\tau)}{r^2(\tau)} d\tau, \quad (14)$$

that is a monotonic increasing function, since h and r represent the magnitude of \vec{h} and \vec{r} , respectively, and Assumption 3.1 prevents them to be zero, so $h, r > 0$. Therefore, A_R will asymptotically converge to $A_R = 0$. In this case, $A_T = 0$ follows from it. ■

Proposition 3.1 is very important, since it allows to control a vector \vec{A} by a single sliding surface. We will make use of it for controlling the osculating plane. As the point to be orbited is already defined by writing the equations of motion, Eqs. 1, in a frame centred on it, the particle's plane is defined by the versor \hat{h} . Therefore, we can make use of this fact to choose a desired specific angular momentum versor \hat{h}_d , defined in RTN using Definition 2.1 as:

$$\hat{h}_{d-RTN} = \begin{bmatrix} h_{dR} \\ h_{dT} \\ h_{dN} \end{bmatrix}, \quad (15)$$

to make \hat{h} converge to it.

Assumption 3.2. Let β be an angle between the desired angular momentum versor \hat{h}_d and the actual angular momentum versor \hat{h} , $\cos \beta = \hat{h} \cdot \hat{h}_d$. The magnitude of this angle is bounded such that $\beta < 90^\circ$.

Now, we are able to derive a control law for controlling the osculating plane, given by the next theorem.

Theorem 1. Assuming that the perturbation normal to the orbit, d_N , is bounded such that $|d_N| < D_N$. A control normal to the osculating plane:

$$u_N = \frac{h^2}{r^3 h_{dN}} (h_{dR} - \lambda_N h_{dT}) - K_N \text{sgn}(s_N) - f_N, \quad (16)$$

$K_N \geq D_N$, will guarantee convergence to the sliding surface:

$$s_N = \hat{h}_d \cdot (\lambda_N \hat{r} + \hat{\theta}) = h_{dT} + \lambda_N h_{dR} = 0, \quad (17)$$

and, once reached, the osculating plane will asymptotically converge to the desired plane defined by \hat{h}_d .

Proof. Taking the derivative of Eq. 17, it follows that:

$$\dot{s}_N = \dot{h}_{dT} + \lambda_N \dot{h}_{dR} \quad (18)$$

Using Eq. 9 and the fact that $\dot{\hat{h}}_d = 0$:

$$\dot{s}_N = \frac{r h_{dN}}{h} a_N + \frac{h}{r^2} (\lambda_N h_{dT} - h_{dR}). \quad (19)$$

Choosing the following Lyapunov candidate:

$$V = \frac{1}{2} s_N^2, \quad (20)$$

we find that:

$$\dot{V} = s_N \dot{s}_N. \quad (21)$$

Because $a_N = f_N + d_N + u_N$:

$$\dot{V} = s_N \left[\frac{r h_{dN}}{h} (f_N + d_N + u_N) + \frac{h}{r^2} (\lambda_N h_{dT} - h_{dR}) \right] \quad (22)$$

Substituting the control u_N given by Eq. 16 we obtain:

$$\dot{V} = \frac{r h_{dN}}{h} s_N (d_N - K_N \text{sgn}(s_N)) \quad (23)$$

The Assumption 3.2 guarantees that $h_{dN} > 0$. Therefore, because $K_N \geq D_N$, and remembering Assumption 3.1, the magnitude of \dot{V} is bounded such that $\dot{V} < 0$ for all $s_N \neq 0$. In this way, we show by the Lyapunov's second method that the system is stable in $s_N = 0$. This implies, using Proposition 3.1, that the osculating plane will asymptotically converge to the desired plane defined by \hat{h}_d , since $\dot{\hat{h}}_d = 0$. ■

Corollary 1.1. *Finite time convergence to the sliding surface s_N , given by Eq. 17, can be obtained by choosing:*

$$u_N = \frac{h^2}{r^3 h_{dN}} (h_{dR} - \lambda_N h_{dT} - K_N \text{sgn}(s_N) - f_N). \quad (24)$$

Remark 1. Note that Assumption 3.2 also prevents u_N from reaching the singularity $h_{dN} = 0$.

Remark 2. In practice, Assumption 3.2 can be circumvented easily in an algorithm that conventionally chooses an intermediary \hat{h}_d if $\beta \geq 90^\circ$.

Remark 3. Note that Theorem 1 decouples the osculating plane by a single sliding surface and control command. This can result in far reaching consequences than the one analysed in this work, as in theory this allows for any planar path following algorithm [25] to be applied after the convergence of the osculating plane given by Theorem 1.

The Proposition 3.1 is a really innovative way of approaching this problem to obtain a control law such as the one in Theorem 1. Let us consider now the angle β defined in Assumption 3.2. One could easily ponder that a sliding surface $s_N = \tilde{\beta} = \beta - \beta_d$ would be a better sliding surface, since it is more intuitive, if an effective robust control can be derived from it.

Deriving $\cos \beta = \hat{h} \cdot \hat{h}_d$, and using Eq. 8, one can find that:

$$\sin \beta \dot{\beta} = 2 \frac{r a_N}{h} h_{dT}. \quad (25)$$

This equation has no dependence on h_{dR} , making the component h_{dR} impossible of being controlled. This is deeper than how the equation is derived or the coordinate system chosen, it has to do with the definition of \hat{h} itself being involved in the sliding surface definition. This can be checked in a broad sense by writing $\cos \beta = \frac{1}{h} \vec{h} \cdot \hat{h}_d$ and deriving it:

$$-\sin \beta \dot{\beta} = \frac{1}{h} \left[(\vec{r} \times \vec{a}) \cdot \hat{h}_d + (\vec{r} \times \vec{v}) \cdot \dot{\hat{h}}_d \right] \quad (26)$$

$$-\frac{\dot{h}}{h} (\vec{r} \times \vec{v}) \cdot \hat{h}_d \Big], \quad (27)$$

in which each term is dependent of the cross product with the position vector. The sliding surface in Eq.

17 is effective in avoiding this drawback by removing \vec{h} from its definition. This can only be obtained using the new sliding surface defined in Proposition 3.1.

So far, a control for the plane was obtained with Theorem 1. Now, it is necessary to derive a control law for the whole geometry of the orbit. A hint for that can be obtained from the constants of motion of the two-body problem. It is known that the specific angular momentum \vec{h} , eccentricity vector¹ \vec{e} and energy E , form five independent constants of motion in the two-body problem, which are the ones defining the geometry of the orbit[13, 7]. The orbital plane control constrained two of these by controlling \hat{h} , so we are left with h , \vec{e} and E . We found that the best combination here is in controlling the specific angular momentum magnitude h and the eccentricity vector²:

$$\vec{e} = \frac{1}{\mu} (\vec{v} \times \vec{h} - \mu \hat{r}), \quad (28)$$

where μ would represent the gravitational parameter in the context of celestial mechanics or astrodynamics, for instance. In the general case, where there is no two-body problem, μ is a design parameter, that can be chosen in different ways, such as defining an orbital period and obtaining μ from the Kepler's third law. Of course, because of the disturbances or practical limitations, the chosen period might not exactly match the one in practice. However, it can be a good approximation offering to the designer a good sense without committing to any trajectory tracking.

It can be shown that the eccentricity vector in RTN coordinates is:

$$\vec{e}_{RTN} = \frac{1}{\mu} \begin{bmatrix} \frac{h^2}{r} - \mu \\ -\dot{r}h \\ 0 \end{bmatrix}, \quad (29)$$

and its time derivative, remembering Definition 2.2,

¹The eccentricity vector is another way of writing the Laplace-Runge-Lenz vector in a way that its magnitude is equivalent to the eccentricity of the orbit.

²For the sake of paper conciseness we will abstain further discussions and proofs regarding the two-body problem, since its solution is well known for centuries and found in any book of classical mechanics, astrodynamics or celestial mechanics [7, 13, 5].

also written in RTN:

$$\dot{\vec{e}}_{RTN} = \frac{1}{\mu} \begin{bmatrix} 2ha_T \\ -ha_R - \dot{r}ra_T - \frac{\mu h}{r^2} \\ -\dot{r}ra_N \end{bmatrix}. \quad (30)$$

With these, we can choose a desired specific angular momentum magnitude h_d and a desired eccentricity vector:

$$\vec{e}_d = \begin{bmatrix} e_{dR} \\ e_{dT} \\ e_{dN} \end{bmatrix}, \quad (31)$$

to derive a robust path following control law of a Keplerian orbit as shown in Theorem 2.

Theorem 2. *Consider the path following control law:*

$$\vec{u}_{RTN} = -F^{-1}(G + K \text{sgn}(\vec{s})) - \vec{f}_{RTN}, \quad (32)$$

where $\vec{u}_{RTN} = [u_R \ u_T \ u_N]^T$, $K \in \mathbb{R}^{3 \times 3}$ is a diagonal positive definite matrix such that its elements are $K_{j,j} \geq \max(|\alpha_j|)$, $j = 1, 2, 3$, for $\vec{\alpha} = F\vec{d}_{RTN}$, the function $\text{sgn}(\vec{s}) \in \mathbb{R}^{3 \times 1}$ represents the sign function taken in each component of \vec{s} , and the matrices F and G are defined by:

$$F = \frac{1}{h\mu} \begin{bmatrix} -h^2 & (2\lambda_R h - \dot{r}r)h & -\mu r e_{dN} \\ 0 & \mu r h & 0 \\ 0 & 0 & \mu r h_{dN} \end{bmatrix}, \quad (33a)$$

$$G = \frac{h}{r^2} \begin{bmatrix} \lambda_R \tilde{e}_T - \tilde{e}_R - 1 \\ 0 \\ \lambda_N h_{dT} - h_{dR} \end{bmatrix}, \quad (33b)$$

$\tilde{e}_R = e_R - e_{dR}$, $\tilde{e}_T = e_T - e_{dT}$, and $\lambda_N, \lambda_R > 0^3$. The control law in Eq. 32 will guarantee convergence to the sliding surface:

$$\vec{s} = \begin{bmatrix} \tilde{e} \cdot (\lambda_R \hat{r} + \hat{\theta}) \\ \tilde{h} \\ \hat{h}_d \cdot (\lambda_N \hat{r} + \hat{\theta}) \end{bmatrix} = 0, \quad (34)$$

$\tilde{h} = h - h_d$, $\tilde{e} = \vec{e} - \vec{e}_d$, and, once reached, will asymptotically converge to the desired orbit geometry defined by \vec{h}_d and \vec{e}_d .

³Note that \dot{r} is the radial velocity, which is simply: $\dot{r} = \vec{v} \cdot \hat{r}$

Proof. Choosing the Lyapunov candidate:

$$V = \frac{1}{2} \vec{s} \cdot \vec{s}, \quad (35)$$

its derivative can be readily obtained:

$$\dot{V} = \vec{s} \cdot \dot{\vec{s}}. \quad (36)$$

Thus, using Eq. 8 and knowing \vec{e}_d and h_d are constants:

$$\dot{V} = \vec{s} \cdot \begin{bmatrix} \dot{\vec{e}} \cdot (\lambda_R \hat{r} + \hat{\theta}) + \tilde{e} \cdot \left(\lambda_R \frac{h}{r^2} \hat{\theta} - \frac{h}{r^2} \hat{r} + \frac{r}{h} a_N \hat{h} \right) \\ \dot{h} \\ \frac{r h_{dN}}{h} a_N + \frac{h}{r^2} (\lambda_N h_{dT} - h_{dR}) \end{bmatrix}, \quad (37)$$

which with Eqs. 6b, 29 and 30, can be written in matrix form as:

$$\dot{V} = \vec{s} \cdot \left(F \vec{f}_{RTN} + F \vec{u}_{RTN} + F \vec{d}_{RTN} + G \right). \quad (38)$$

One can easily check that F is a non-singular matrix. Because K can be chosen such that $K_{j,j} \geq \max(|\alpha_j|)$, $j = 1, 2, 3$, for $\vec{\alpha} = F\vec{d}_{RTN}$, one find by applying Eq. 32 that $\dot{V} < 0$. Therefore, the system is asymptotically stable in $\vec{s} = 0$.

On the sliding surface, the second element of the sliding surface vector, \vec{s} , only admits the solution $h = h_d$. The third element will converge asymptotically as already shown in Theorem 1. Lastly, the first element can be shown to converge to \vec{e}_d by using Eqs. 9 and 30 to rewrite it as:

$$\dot{\tilde{e}}_R = \frac{2h}{\mu} a_T - \lambda_R \dot{\theta} \tilde{e}_R. \quad (39)$$

Using Filippov's Method [24, 26] we can make $\dot{\vec{s}} = 0$ to find that the equivalent \vec{u}_{RTN} is:

$$\vec{u}_{RTN-eq} = -F^{-1}G. \quad (40)$$

In solving Eq. 40 one will find that the transverse component a_{T-eq} is equal zero. Therefore, following Eq. 12 in Proposition 3.1, the radial and transverse components of \vec{e} will asymptotically converge to zero. Meanwhile, the normal component \tilde{e}_N will converge to zero following the asymptotic convergence of the orbital plane, since when the orbital plane converges ($\hat{h} = \hat{h}_d$) the vectors \vec{e} and \vec{e}_d will have only radial and transverse components, as they are perpendicular to \hat{h} and \hat{h}_d [7, 13, 5], respectively. ■

Corollary 2.1. *If the components of the disturbance \vec{d}_{RTN} are bounded such that $|d_R| < D_R$, $|d_T| < D_T$, and $|d_N| < D_N$, each element of the diagonal matrix K can be chosen, while still guaranteeing stability of Theorem 2, accordingly to:*

$$K_{1,1} \geq \frac{h}{\mu} D_R + \left| \frac{2\lambda_R h - \dot{r}r}{\mu} \right| D_T + \frac{r|e_{dN}|}{h} D_N, \quad (41a)$$

$$K_{2,2} \geq r D_T, \quad (41b)$$

$$K_{3,3} \geq r \frac{h_{dN}}{h} D_N. \quad (41c)$$

Proof. Following the definition of $\vec{\alpha}$ in Theorem 2, $\vec{\alpha} = F\vec{d}_{RTN}$, we obtain:

$$\vec{\alpha} = \begin{bmatrix} -\frac{h}{\mu} d_R + \frac{2\lambda_R h - \dot{r}r}{\mu} d_T - \frac{1}{h} r e_{dN} d_N \\ r d_T \\ r \frac{h_{dN}}{h} d_N \end{bmatrix}, \quad (42)$$

because $K_{j,j} \geq \max(|\alpha_j|)$, it easily follows that $K_{2,2} \geq r D_T$ and $K_{3,3} \geq r \frac{h_{dN}}{h} D_N$. For the radial component α_R , the following bounds are true:

$$\alpha_R \leq \frac{h}{\mu} D_R + \left| \frac{2\lambda_R h - \dot{r}r}{\mu} \right| D_T + \frac{r|e_{dN}|}{h} D_N = \alpha_R^+, \quad (43a)$$

$$\alpha_R \geq -\frac{h}{\mu} D_R - \left| \frac{2\lambda_R h - \dot{r}r}{\mu} \right| D_T - \frac{r|e_{dN}|}{h} D_N = \alpha_R^-. \quad (43b)$$

Therefore, since $\alpha_R^+ = -\alpha_R^-$, it follows that $\max(|\alpha_R|) \leq \alpha_R^+$, and $K_{1,1}$ can then be safely chosen respecting the bound: $K_{1,1} \geq \alpha_R^+$. ■

It is widely known that the main drawback of the sliding mode is its discontinuous control input, which in many practical applications lead to chattering. This can be easily dealt with by allowing the system to converge to a boundary around the sliding surface, at the expense of a little performance, as extensively documented in the literature [24, 26]. The most common approach is to substitute the sign function by the saturation function:

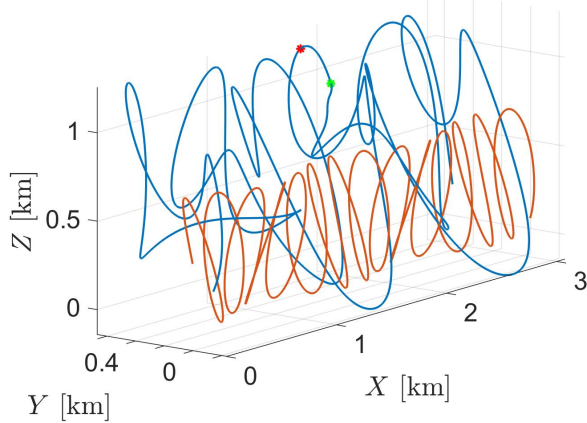
$$\text{sat}(s_j, \Phi_j) = \begin{cases} 1, & s_j > \Phi_j \\ \frac{s_j}{\Phi_j}, & -\Phi_j \leq s_j \leq \Phi_j \\ -1, & s_j < -\Phi_j \end{cases}. \quad (44)$$

In this way, we can replace the $\text{sgn}(\vec{s})$ in Eq. 32 by $\text{sat}(\vec{s}, \vec{\Phi})$, representing the saturation function of Eq. 44 taken in each component of \vec{s} for the corresponding component of $\vec{\Phi}$.

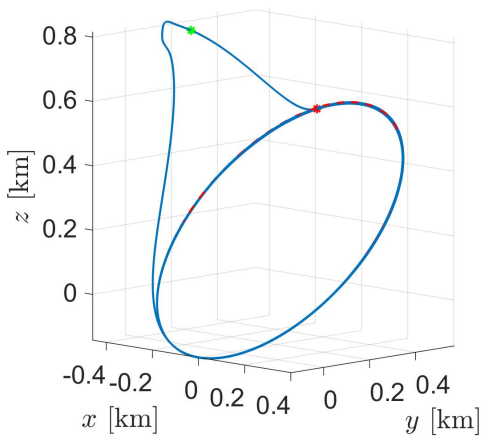
4 Illustrative Examples

Our first example is a moving path following (MPF) problem. In this example, we seek to be the more general as possible to show the extension of applicability of the proposed path following law, without committing to any specific application. The particle is requested to orbit a point that moves in a sinusoidal trajectory with velocity $\vec{V} = [5 \quad \frac{5}{3} \cos(\frac{t}{6}) \quad 50 \cos(\frac{t}{7})]^\top$ m/s in an inertial frame. The particle's desired specific angular momentum and eccentricity vectors, relative to the moving point, are: $\vec{h}_d = [0 \quad -8,885.8 \quad 8,885.8]^\top$ m²/s and $\vec{e}_d = [0 \quad -0.4243 \quad -0.4243]^\top$. In this example, we will consider that all the forces but the control are disturbances, which include terms of the accelerated point and a constant acceleration of magnitude $[0 \quad 0 \quad -3]^\top$ m/s². Moreover, to stress the path following law, we consider that the particle loses all of its control commands for 15 seconds during the simulation and that the control components are saturated by 20 m/s² in each inertial frame direction, so that it has to recover the path after that. The gain matrix K is calculated following the equality in Corollary 2.1, for $D_R = D_T = D_N = 10$ m/s², the vector $\vec{\Phi}$ is chosen as 5% of each element of the matrix K , and $\lambda_R = \lambda_N = 2$. The parameter μ is obtained by choosing an orbital period of 100 seconds, and solving the Kepler's third law. Figures 1 and 2 show the results obtained for this case for a 10 minutes simulation. The moving point trajectory is represented in orange in Fig. 1a, representing the trajectory in the inertial frame, while the particle's trajectory is depicted in blue in Figs. 1a and 1b, with the last representing the orbit relative to the moving point. A red asterisk represents the point of the trajectory where the particle loses the control commands, while the green one depict the point where they are back, showing that the control law is effective in recovering

the trajectory. In Fig. 2, one can check the moment which the control command is turned off (6 minutes) and the prompt reaction of the control for recovering the path after turned back on. One can also check, in Fig. 2, that the saturation function in Eq. 44 is effective in removing the chattering with negligible loss of performance, as shown in Fig. 1b by the perfect match of the particle's orbit with the desired path (depicted as a red dashed line, barely noticeable due to the high performance of the control law).



(a) Inertial frame



(b) Frame centred in the orbited point

Figure 1: Controlled orbit for the MPF example.

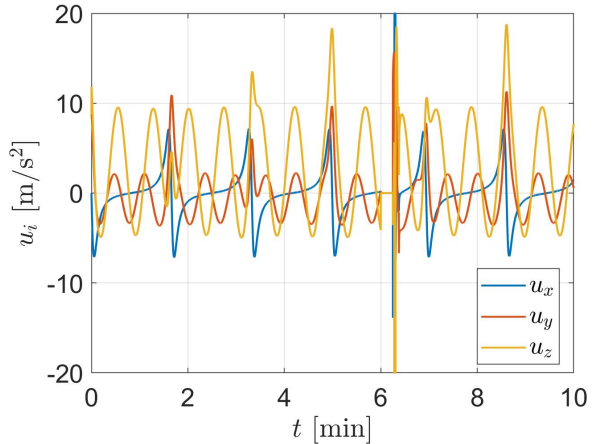


Figure 2: The control Cartesian components for the MPF example.

The control law can achieve any conic section. Figures 3 and 4 show an example using hyperboles. In this example the particle is requested to describe a hyperbole relative to three different checkpoints, accordingly to which of them is closest. A possible application of this could be for an UAV that performs line transmission inspection. Figure 3 represents the trajectory of the particle in an inertial frame, with each checkpoint and its respective hyperbole represented in red. We choose to make all hyperboles on the plane for a better visualization. Here, it is also considered that $D_R = D_T = D_N = 10 \text{ m/s}^2$, Φ is 5% of the diagonal of K , and $\lambda_R = \lambda_N = 2$. As disturbance we consider an acceleration $\vec{d} = [5 \sin(t) \quad 5 \cos(t/3) \quad -3 + 5 \sin(t/5)]^T \text{ m/s}^2$. Figure 4 shows the control components. Note in Fig. 3 that the desired hyperboles' legs are severely mismatched, this is on purpose to stress the control law. However, in practical applications, the hyperboles would be conventionally chosen to almost match their legs for a smooth transition between different checkpoints.

The last example is a more specific one, that is the autonomous orbit keeping problem, using the asteroid Itokawa, to control an orbit that corresponds to $\vec{h}_d = [28.4818 \quad 0 \quad 0]^T \text{ m}^2/\text{s}$ and $\vec{e}_d = [0 \quad 0 \quad 0.1]^T$. We consider as disturbances the solar radiation pres-

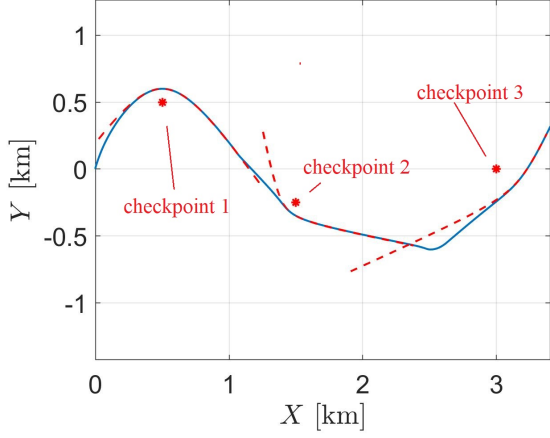


Figure 3: Patched hyperboles example in the inertial frame.

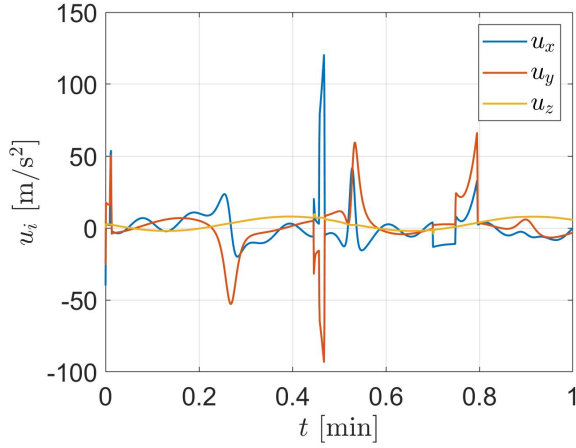


Figure 4: The control Cartesian components for the patched hyperboles example.

sure, with parameters $S = 1.695$ AU, $B_{sc} = 20$ kg/m² and $\rho = 1$ (following the definitions in [17]), the unknown asteroid's spin state, and higher-order terms of the gravity field, obtained by the polyhedron model of [28]. So the only known force is the main gravity term. Figures 5 to 6 show the results for a 24h simulation in the inertial frame. Matrix K is chosen for $D_R = D_T = D_N = 10^{-4}$ m/s², $\vec{\Phi}$ is 5 times each

element of the diagonal of K , and $\lambda_R = \lambda_N = 2$. As shown in Fig. 5, the orbit is successfully maintained. If no control input is applied, the spacecraft would escape Itokawa in only 3 hours, after a close approach with one of the rotating asteroid's lobes. One can note in Figure 4, which represents the control commands in the Cartesian coordinates, that the saturation function is successful in avoiding chattering. The total ΔV for this 24 hour operation is only 1.2211 m/s. For more details on the modelling specificities and the advantages of our path following law for the orbit keeping problem, we refer the reader to [17], where a focused analysis of the orbit keeping problem is done, considering its multiple practical aspects.

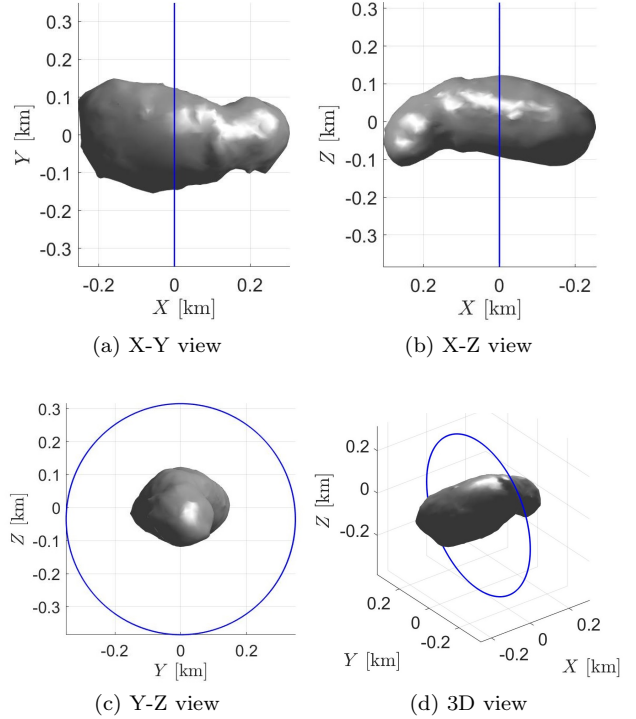


Figure 5: Controlled orbit around Itokawa, in the inertial frame.

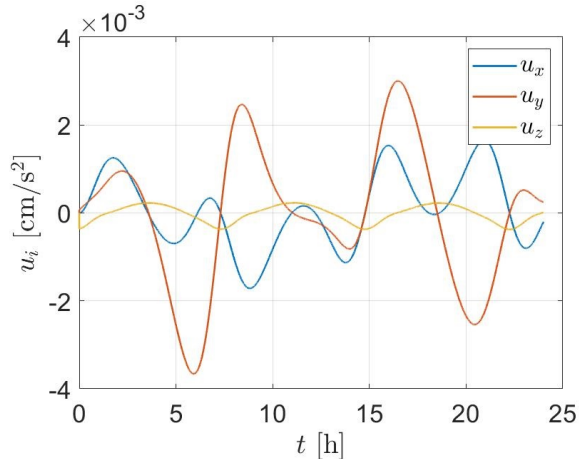


Figure 6: The control Cartesian components for the Itokawa example.

5 Conclusions

In this work, we proposed and proved asymptotic convergence of a novel path following law that takes advantage of the structure of the solution of the two-body problem to constrain any Keplerian orbit. This was done under a robust control frame, explicitly dealing with bounded disturbances, in which we choose to apply sliding mode control theory. To this end, we proposed and proved asymptotic convergence of a novel kind of sliding surface, written as a linear combination of radial and transverse components of an arbitrary vector, which allows to control a vector through a single sliding surface. A consequence of this is in decoupling the osculating plane control in a single control command and sliding surface, which could be the basis for further studies considering different frameworks for the on the plane control, possibly mixing with the abundant 2D path following algorithms in the literature. Our work could be an inspiration in further theoretical studies for the elaboration of different constrains that could produce non-Keplerian motion. In this case, our proposed sliding surface is also an important theoretical tool. We exemplify the far range of applicability of this novel path following using three stringent applications. One for a general moving path following prob-

lem, which shows the potential application of this control strategy for problems in which an aerial or underwater vehicle is requested to orbit a point which is a projection of the path followed by a car or ship into certain altitude or depth. Secondly, we present a patched hyperboles problem, that could be thought as a representation of an UAV line transmission inspection task. The last example is an autonomous orbit keeping problem around the asteroid Itokawa, in which a spacecraft is request to keep its orbit in a highly perturbed environment. For all of these, we consider that the proposed path following control have further implications in theoretical and applied research.

Acknowledgements

The authors wish to express their appreciation for the support provided by grants # 406841/2016-0 and 301338/2016-7 from the National Council for Scientific and Technological Development (CNPq); grants # 2017/20794-2, 2015/19880-6 and 2016/24561-0 from São Paulo Research Foundation (FAPESP) and the financial support from the Coordination for the Improvement of Higher Education Personnel (CAPES).

References

- [1] A Pedro Aguiar, Dragan B Dačić, Joao P Hespanha, and Petar Kokotović. Path-following or reference tracking?: An answer relaxing the limits to performance. *IFAC Proceedings Volumes*, 37(8):167–172, 2004.
- [2] A Pedro Aguiar and Joao P Hespanha. Trajectory-tracking and path-following of under-actuated autonomous vehicles with parametric modeling uncertainty. *IEEE transactions on automatic control*, 52(8):1362–1379, 2007.
- [3] A Pedro Aguiar, Joao P Hespanha, and Petar V Kokotovic. Path-following for nonminimum phase systems removes performance limita-

- tions. *IEEE Transactions on Automatic Control*, 50(2):234–239, 2005.
- [4] A Pedro Aguiar, João P Hespanha, and Petar V Kokotović. Performance limitations in reference tracking and path following for nonlinear systems. *Automatica*, 44(3):598–610, 2008.
- [5] Vladimir I Arnold, Valery V Kozlov, and Anatoly I Neishtadt. *Mathematical aspects of classical and celestial mechanics*, volume 3. Springer Science & Business Media, 2007.
- [6] Andrzej Banaszuk and John Hauser. Feedback linearization of transverse dynamics for periodic orbits. *Systems & control letters*, 26(2):95–105, 1995.
- [7] Richard H Battin. *An introduction to the mathematics and methods of astrodynamics, revised edition*. American Institute of Aeronautics and Astronautics, 1999.
- [8] Dennis Belleter, Mohamed Adlene Maghenem, Claudio Paliotta, and Kristin Y Pettersen. Observer based path following for underactuated marine vessels in the presence of ocean currents: A global approach. *Automatica*, 100:123–134, 2019.
- [9] Even Børhaug, Alexey Pavlov, Elena Panteley, and Kristin Y Pettersen. Straight line path following for formations of underactuated marine surface vessels. *IEEE transactions on control systems technology*, 19(3):493–506, 2010.
- [10] Luca Consolini, Manfredi Maggiore, Christopher Nielsen, and Mario Tosques. Path following for the pvtol aircraft. *Automatica*, 46(8):1284–1296, 2010.
- [11] Thor I Fossen, Morten Breivik, and Roger Skjetne. Line-of-sight path following of underactuated marine craft. *IFAC proceedings volumes*, 36(21):211–216, 2003.
- [12] Andrea Garulli, Antonio Giannitrapani, Mirko Leomanni, and Fabrizio Scortecchi. Autonomous low-earth-orbit station-keeping with electric propulsion. *Journal of guidance, control, and dynamics*, 34(6):1683–1693, 2011.
- [13] Herbert Goldstein, Charles Poole, and John Safko. *Classical mechanics*. Pearson Education Limited, third edition, 2014.
- [14] J-M Kai, Tarek Hamel, and Claude Samson. A unified approach to fixed-wing aircraft path following guidance and control. *Automatica*, 108:108491, 2019.
- [15] Yuri A Kapitanyuk, Anton V Proskurnikov, and Ming Cao. A guiding vector-field algorithm for path-following control of nonholonomic mobile robots. *IEEE Transactions on Control Systems Technology*, 26(4):1372–1385, 2017.
- [16] Eleni Kelasidi, Pål Liljebäck, Kristin Y Pettersen, and Jan Tommy Gravdahl. Integral line-of-sight guidance for path following control of underwater snake robots: Theory and experiments. *IEEE Transactions on Robotics*, 33(3):610–628, 2017.
- [17] RB Negri and AFBA Prado. Autonomous and robust orbit keeping for small body missions. *Submitted to Journal of Guidance, Control, and Dynamics*, 2020.
- [18] Derek R Nelson, D Blake Barber, Timothy W McLain, and Randal W Beard. Vector field path following for miniature air vehicles. *IEEE Transactions on Robotics*, 23(3):519–529, 2007.
- [19] Christopher Nielsen, Cameron Fulford, and Manfredi Maggiore. Path following using transverse feedback linearization: Application to a maglev positioning system. *Automatica*, 46(3):585–590, 2010.
- [20] Christopher Nielsen and Manfredi Maggiore. On local transverse feedback linearization. *SIAM Journal on Control and Optimization*, 47(5):2227–2250, 2008.
- [21] Tiago Oliveira, A Pedro Aguiar, and Pedro Encarnação. A convoy protection strategy using the

- moving path following method. In *2016 International Conference on Unmanned Aircraft Systems (ICUAS)*, pages 521–530. IEEE, 2016.
- [22] Tiago Oliveira, A Pedro Aguiar, and Pedro Encarnacao. Moving path following for unmanned aerial vehicles with applications to single and multiple target tracking problems. *IEEE Transactions on Robotics*, 32(5):1062–1078, 2016.
- [23] Tiago Oliveira, Pedro Encarnação, and A Pedro Aguiar. Moving path following for autonomous robotic vehicles. In *2013 European Control Conference (ECC)*, pages 3320–3325. IEEE, 2013.
- [24] Jean-Jacques E Slotine, Weiping Li, et al. *Applied nonlinear control*, volume 199. Prentice hall Englewood Cliffs, NJ, 1991.
- [25] PB Sujit, Srikanth Saripalli, and Joao Borges Sousa. Unmanned aerial vehicle path following: A survey and analysis of algorithms for fixed-wing unmanned aerial vehicles. *IEEE Control Systems Magazine*, 34(1):42–59, 2014.
- [26] Vadim Utkin, Jürgen Guldner, and Jingxin Shi. *Sliding mode control in electro-mechanical systems*. CRC press, 2017.
- [27] Yuanzhe Wang, Danwei Wang, and Senqiang Zhu. Cooperative moving path following for multiple fixed-wing unmanned aerial vehicles with speed constraints. *Automatica*, 100:82–89, 2019.
- [28] Robert A Werner and Daniel J Scheeres. Exterior gravitation of a polyhedron derived and compared with harmonic and mascon gravitation representations of asteroid 4769 castalia. *Celestial Mechanics and Dynamical Astronomy*, 65(3):313–344, 1996.
- [29] C Canudas de Wit, Hayate Khenouf, Claude Samson, and Ole J Sordalen. Nonlinear control design for mobile robots. In *Recent trends in mobile robots*, pages 121–156. World Scientific, 1993.
- [30] Xinyu Wu, Jia Liu, Chenyang Huang, Meng Su, and Tiantian Xu. 3-d path following of helical microswimmers with an adaptive orientation compensation model. *IEEE Transactions on Automation Science and Engineering*, 17(2):823–832, 2019.
- [31] Weijia Yao and Ming Cao. Path following control in 3d using a vector field. *Automatica*, 117:108957, 2020.
- [32] Zewei Zheng. Moving path following control for a surface vessel with error constraint. *Automatica*, 118:109040, 2020.
- [33] Zongyu Zuo, Lin Cheng, Xinxin Wang, and Kangwen Sun. Three-dimensional path-following backstepping control for an under-actuated stratospheric airship. *IEEE Transactions on Aerospace and Electronic Systems*, 55(3):1483–1497, 2018.